Distributed Acoustic Sensing Using an Ultra-stable Laser

A Thesis

submitted to
Indian Institute of Science Education and Research Pune
in partial fulfillment of the requirements for the
BS-MS Dual Degree Programme

by

Sumit Ghosh

Indian Institute of Science Education and Research Pune
Dr. Homi Bhabha Road,
Pashan, Pune 411008, INDIA.

April, 2025

Supervisor: Prof. Subhadeep De

Certificate

This is to certify that this dissertation entitled "Distributed Acoustic Sensing Using an Ultra-stable Laser" submitted towards the partial fulfilment of the BS-MS dual degree programme at the Indian Institute of Science Education and Research (IISER), Pune represents study/work carried out by Sumit Ghosh at Inter-University Center for Astronomy and Astrophysics (IUCAA) under the supervision of Prof. Subhadeep De, Associate Professor, during the academic year 2024-2025.

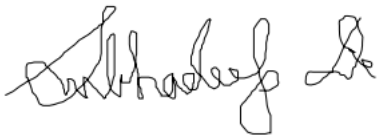

Prof. Subhadeep De

Committee:

Prof. Subhadeep De

Prof. Atikur Rahman

Dedicated to my parents.

Declaration

I hereby declare that the matter embodied in the report entitled "Distributed Acoustic Sensing Using an Ultra-stable Laser" are the results of the investigation carried out by me at the, Inter-University Center for Astronomy and Astrophysics (IUCAA), under the supervision of Prof. Subhadeep De and the same has not been submitted elsewhere for any other degree. Wherever others contribute, every effort is made to indicate this clearly, with due reference to the literature and acknowledgement of collaborative research and discussions.

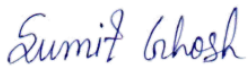

Sumit Ghosh

Acknowledgments

I sincerely thank my supervisor, Prof. Subhadeep De, for his invaluable guidance, mentorship, and patience throughout this project. His insights have been instrumental in shaping my research. I am also grateful to Prof. Atikur Rahman (IISER Pune) for his constant support and encouragement.

I deeply appreciate my research group members—Stanley, Sujaya, Sankalpa, Sankar, and Venu—for their insightful discussions and collaboration. Special thanks to my parents for their unwavering support and to my friends—Harsh, Mayank, Priyanshu, Ayush, Ridham, Harshit, and Gaurav—for their motivation and companionship.

I extend my gratitude to the Director and administration of IUCAA, Pune, for facilitating my research and to the IUCAA computer section, especially Prafull Barathe, for their technical assistance. I also thank the I-Hub Quantum Technology Foundation for awarding me the Chanakya Undergraduate Fellowship (2024–25).

Finally, I acknowledge everyone who has contributed to my academic journey. Your support has been truly invaluable.

Abstract

Distributed Acoustic Sensing (DAS) technology, which utilizes optical fibres to monitor vibrations and acoustic signals, has emerged as a powerful tool for applications ranging from structural health monitoring of bridges and pipelines to geophysical exploration and surveillance. This study investigates using an ultra-narrow linewidth ultra-stable continuous-wave (CW) laser operating at a wavelength of 1550 nm to enhance the performance and reliability of fiber-based DAS systems. The proposed system addresses the limitations of phase noise and frequency instability, delivering improved signal-to-noise ratio (SNR) and detection sensitivity. The CW laser, characterized by exceptional coherence properties, continuously interrogates the optical fibre, which serves as both the sensing element and the transmission medium. Environmental perturbations such as acoustic waves or vibrations induce phase changes in the fibre, which are captured through a beat-note signal between the stable laser and the propagated light. These variations are processed to accurately detect and localize disturbances with a spatial resolution of $\pm 5\,\mathrm{m}$. The system can detect frequencies from $< 0.01\,\mathrm{Hz}$ up to $500\,\mathrm{Hz}$. This system can be used for acceleration sensitivity/mass movement at peak-particle velocities (PPV) of sub-µm/s. By minimizing phase noise, the ultra-stable laser source ensures precise and reliable measurements, demonstrating significant potential for applications such as validating acoustic vibrations in gravitational wave detectors. The findings highlight the transformative impact of integrating ultra-narrow ultra-stable CW lasers into DAS systems, paving the way for advancements in acoustic sensing technologies across various industries with enhanced accuracy, sensitivity, and spatial resolution.

Contents

List of Figures

Chapter 1

Introduction

"All our knowledge has its origins in our perceptions."
– *Leonardo da Vinci*

The advancement of modern science heavily relies on the continuous improvement of research equipment and the creation of innovative tools that expand our understanding of the world. A key challenge in this progress is integrating state-of-the-art research instruments and techniques into scientific fields where they have yet to be utilized. Fibre-based sensors represent one of the most advanced families of modern measurement instruments, as clearly described by Fang et al. [1]. While conventional telecommunication optical fibres are widely used, specialized optical fibres have also been developed for sensing applications. Compared to electrical sensors, fibre-optic sensors offer several advantages, including their lightweight nature, compact size, electricity-free sensing elements, and immunity to electromagnetic interference and harsh environments [2]. These features enable their use in hazardous conditions such as explosive atmospheres, combustible mixtures [3], and strong electromagnetic fields.

Among fibre-optic sensors, distributed fibre sensors stand out as a significant technological advancement in metrology and scientific research. Their capabilities and advantages have been extensively demonstrated by A. Hartog [4]. These sensors have been rapidly adopted in various research fields, providing solutions to numerous practical challenges. Their key strength lies in their ability to obtain spatially resolved information, as an optical fibre or cable can be positioned around an entire structure or volume to capture distributed mea-

surements. A typical distributed fibre sensing system consists of a sensing element-typically an optical fibre, and an interrogator responsible for generating the optical probe signal and analysing the scattered response within the fibre-based sensor [1, 4]. The ability of distributed sensors to perform localized measurements of physical parameters makes them a highly effective tool for monitoring large-scale structures. Due to this capability, they offer a promising alternative to conventional point-based sensor arrays, as a single optical fibre can replace thousands of individual sensors, simplifying both the measurement setup and the interrogation process [4–6]. The principle of distributed sensing relies on three primary types of scattering that occur within an optical fibre-Rayleigh, Brillouin, and Raman scattering [1, 4, 7]. The scattered light exhibits variations in characteristics such as amplitude, frequency, and polarization, which are influenced by the physical parameters being monitored.

Distributed fibre sensors are used to measure the distribution of various parameters such as temperature [8–15], stress and deformations [16–18], or vibro-acoustic properties [19–24] in different objects. These sensors provide more comprehensive data than static measurements like temperature or stress by also capturing the frequency of variations. The sound emitted by an object or event, also known as its acoustic field or "sound image," offers valuable insights, as almost every event or phenomenon has a unique sound associated with it [25].

1.1 Distributed Acoustic Sensing (DAS)

Fibre-based Distributed Acoustic Sensors (DAS) are effective tools for analyzing these acoustic fields along the fibre's length, essentially functioning as a distributed microphone. DAS technology has been quickly commercialized and is used across various industries. One of the most common applications of DAS is perimeter security [26–28], such as at airports [29], railways [30], power plants, and other critical locations. Typical features of DAS security systems include a fibre length of up to 100 km, fault detection accuracy within 10 m, a frequency sensitivity range from 0.5 Hz to 20 kHz (depending on fibre length), and deformation sensitivity under 1 nϵ. Another significant industrial application of DAS is in geophysics [31, 32]. This method, first introduced 13 years ago [33], has seen continuous growth in usage. DAS is employed in seismic data acquisition, including vertical seismic profiling [34–37], microseismic measurements [38, 39], and monitoring of hydraulic fracturing processes[40–42]. DAS systems can also be used for near-surface characterization of land and subsurface

imaging in boreholes [43], offering an alternative to traditional geophones commonly used in the industry. A key advantage of DAS over geophones is its larger dynamic range at low frequencies.

Ongoing advancements in DAS systems have contributed to their growing popularity, providing solutions for specific challenges. For example, DAS can monitor ocean and solid earth phenomena in marine geophysics, as demonstrated by Hartog et al. [44]. Existing subsea cables (dark fibres) can serve as the sensing elements in these applications, enabling the tracking of sea-state dynamics during storm cycles. Additionally, DAS technology is used to monitor crack formation in materials within buildings, structures, and vehicles. It can measure distributed strains, deflections, and crack widths in reinforced concrete structures [45, 46], aiding in the prevention of costly reconstructions and helping to optimize future designs.

Thus, looking at the importance of DAS in the modern era of sensor physics and technology, we take an innovative approach to its study. In this thesis, we delve into the potential use of an ultra-stable, ultra-narrow linewidth continuous wave laser for DAS. Also, we are interested in the core laser going through the fibre without relying on any scattering phenomena. The layout of this is as follows: the introduction to DAS in Chapter 1. Chapter 2 gives the theoretical model used in the experiment design along with the signal processing techniques and how acoustic vibrations get coupled to the laser. In chapter 3, we describe the experimental setup and data processing techniques. This is followed by the chapter 4, where we have simulated many experimental ideas to get a better view of our setup's advantages. Next, in chapter 5, we provide a detailed analysis of our system. Finally, in chapter 6, we conclude the work with a comparison with other instruments and areas where our system is applicable.

Chapter 2

Theory

2.1 Coupling of Acoustic Sources With Laser

Acoustic waves propagate through a dense medium by inducing pressure variations that cause local particle displacements. These pressure variations manifest as density waves travelling through the medium [47]. When an optical fibre is exposed to such an acoustic wave, it experiences microscopic strain fluctuations due to the elastic properties of the fibre material [48]. This strain alters the optical path length (OPL) in two primary ways:

1. **Physical length change (ΔL)**: The strain induces small elongations or contractions in the fibre length, modifying the effective propagation distance of light.
2. **Refractive index change (Δn)**: The strain alters the refractive index due to the photoelastic effect [49].

The total optical path length variation can be expressed as:

$$\Delta OPL = (n + L\frac{dn}{dL})\Delta L + L\Delta n, \tag{2.1}$$

where n is the refractive index of the fiber, and L is its original length.

These perturbations in the OPL induce phase modulation of the laser propagating through

the fibre. The phase change $\Delta\Phi$ is given by:

$$\Delta\Phi = \frac{2\pi}{\lambda}\Delta OPL, \tag{2.2}$$

Where λ is the laser wavelength. Consequently, the frequency of the laser undergoes a Doppler shift, given by:

$$\Delta f = -\frac{1}{2\pi}\frac{d\Phi}{dt}. \tag{2.3}$$

This effect enables acoustic perturbations to modulate the laser frequency and phase. Since the information propagates along the fibre at the speed of light, optical fibres can serve as sensitive detectors for acoustic disturbances in their surroundings. Such interactions are exploited in distributed acoustic sensing (DAS) applications, where optical fibres detect and localize acoustic events with high precision [4].

2.2 The Mathematical Model

We assume our source (S) to be sinusoidally vibrating with a monochromatic frequency f_S and localized at a fixed point X along the length of the fibre, and we devise a model to retrieve the strength, frequency and location of the source. The schematic of the model is depicted in figure 2.1.

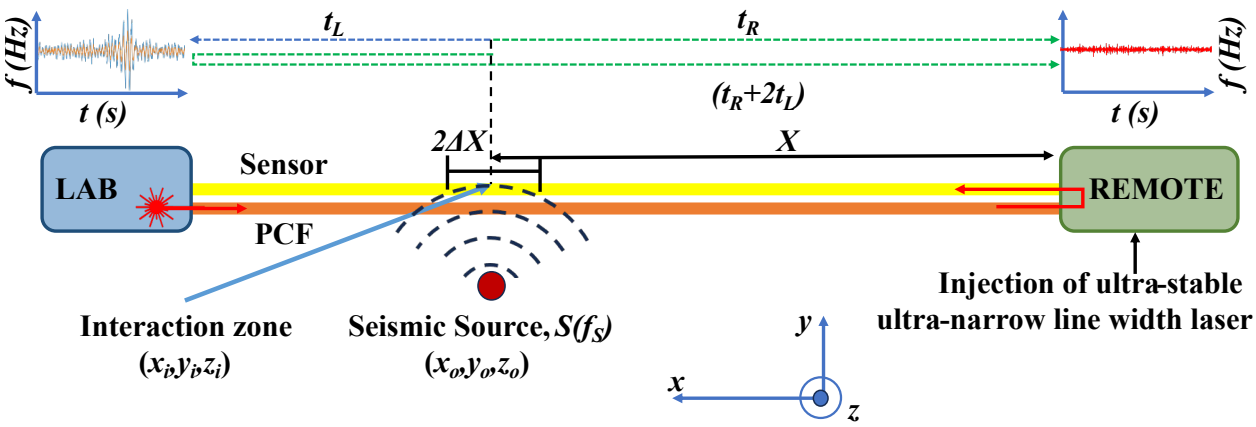

Figure 2.1: Schematic Model of Our DAS: In-loop path shown in green and out-of-loop path shown in blue dashed lines.

We define two paths, in-loop: from source (S) to remote and from source to the lab to remote, the green dashed path as can be viewed in figure 2.1, and out-of-loop: source to the lab, the blue dashed line. The acoustic source, S of frequency f_S, travels along the length of the fibre and reaches the lab and remote where it can be detected.

We find the wave parameters (strength/ amplitude, frequency and phase) from the sine waves detected at these two ends. Let the amplitude of the sine wave generated due to the acoustic source be A, and the time the wave takes to propagate from S to lab is t_L, and from S to remote, it is t_R.

We have two sine waves meeting at remote, from source to remote: $A \sin 2\pi f_S(t - t_R)$ and from source to the lab and looping back to remote: $A \sin 2\pi f_S(t - (t_R + 2t_L))$ (in-loop). And one sine wave reaching the lab from S: $A \sin 2\pi f_S(t - t_L)$. Again, as the acoustic vibrations are coupled to the laser, as discussed in section 2.1, and travelling at the speed of light, we consider no decay in their amplitude due to propagation.

Thus, the combined wave that reaches the remote location is -

$$A \sin 2\pi f_S(t - t_R) + A \sin 2\pi f_S(t - (t_R + 2t_L)) \tag{2.4}$$

Factoring out the common terms, we get:

$$2A \sin 2\pi f_S(t - (t_R + t_L)) \cos(2\pi f_S t_L) \tag{2.5}$$

And the wave reaching the Lab is -

$$A \sin 2\pi f_S(t - t_L) \tag{2.6}$$

From equation 2.5, we get that the strength of the wave reaching the remote end is double, and the term contains only one time-varying factor carrying the phase information: $\sin 2\pi f_S(t - (t_R + t_L))$

Thus, the phase difference between waves equation 2.5 and equation 2.6 is given by:

$$\Delta\phi = 2\pi f_S(t - t_L) - 2\pi f_S(t - t - (t_R + t_L)) = 2\pi f_S t_R \tag{2.7}$$

Thus, finding $\Delta\phi$ indirectly gives us the time information t_R and knowing that the wave

propagates through the fibre at the speed of light, C_{fibre}, we can find the position of the source X as follows -

$$X = c_{\text{fiber}} \cdot t_A \tag{2.8}$$

Substituting for t_A in terms of $\Delta\phi$ from equation 2.7 we get:

$$X = \frac{c_{\text{fiber}}}{2\pi f_s} \cdot \Delta\phi \tag{2.9}$$

2.3 Signal Processing

Signal processing is one of the fundamental disciplines in engineering and physics that deals with the analysis, manipulation, and transformation of signals. In the context of laser frequency stability and noise analysis, signal processing techniques help in extracting meaningful information from measured data. This section provides an overview of essential signal processing techniques used in the analysis of frequency stability and noise characterization.

2.3.1 Fourier Transform and Spectral Analysis

The Fourier Transform (FT) [50] is a powerful mathematical tool that decomposes a signal into its constituent frequencies. It is defined as:

$$X(f) = \int_{-\infty}^{\infty} x(t) e^{-j2\pi ft} dt. \tag{2.10}$$

The Discrete Fourier Transform (DFT) is commonly computed using the Fast Fourier Transform (FFT) algorithm, which efficiently computes the transformation with a complexity of $O(N \log N)$.

Inverse Fourier Transform (IFT) is used to reconstruct a time-domain signal from its frequency-domain representation:

$$x(t) = \int_{-\infty}^{\infty} X(f) e^{j2\pi ft} df. \tag{2.11}$$

FFT and IFFT are widely used in signal analysis, noise characterization, and filtering.

2.3.2 Hilbert Transform and Signal Envelope

The Hilbert Transform is used to obtain the analytic signal, which provides information about the instantaneous amplitude and phase of a signal. It is defined as:

$$\mathcal{H}\{x(t)\} = \frac{1}{\pi} \int_{-\infty}^{\infty} \frac{x(\tau)}{t-\tau} d\tau. \tag{2.12}$$

The analytic signal is then given by:

$$z(t) = x(t) + j\mathcal{H}\{x(t)\}. \tag{2.13}$$

This representation is useful in demodulation and phase analysis [51].

2.3.3 Phase Unwrapping

Phase unwrapping is a technique used to reconstruct the true phase of a signal when it is wrapped within a principal interval, such as $-\pi$ to π. The process ensures continuity in phase measurements, particularly important in interferometry and spectral analysis [52]. By resolving phase ambiguities, unwrapping allows for extracting meaningful physical information from wrapped phase data. Various algorithms, such as path-following and minimum-norm methods, are employed to achieve robust unwrapping, depending on the noise level and signal characteristics. Accurate phase unwrapping is crucial in applications like synthetic aperture radar (SAR) imaging, optical metrology, and laser interferometry, where precise phase information directly impacts measurement accuracy.

2.3.4 Gaussian Filtering

Gaussian filtering is a smoothing technique that applies a Gaussian kernel to a signal or image. The Gaussian filter in one dimension is given by:

$$G(t) = \frac{1}{\sqrt{2\pi\sigma^2}} e^{-\frac{t^2}{2\sigma^2}}. \tag{2.14}$$

This filter is widely used for noise reduction and signal smoothing [53].

2.3.5 Short-Time Fourier Transform and Spectrograms

The Short-Time Fourier Transform (STFT) extends the Fourier Transform by analyzing localized sections of a signal, providing a time-frequency representation. It is defined as:

$$X(t, f) = \int_{-\infty}^{\infty} x(\tau) w(\tau - t) e^{-j2\pi f \tau} d\tau, \tag{2.15}$$

where $w(\tau)$ is a window function. The STFT is used to generate spectrograms and waterfall diagrams, visualizing how the frequency content of a signal evolves over time [54].

Chapter 3

Experiment

3.1 Experimental setup

From the mathematical model discussed in section 2.2, we have to retrieve the in-loop and out-of-loop sine waves for an acoustic source present along the length of the fibre with our experimental setup.

The experimental setup consists of two major components - the phase-coherent optical fibre link (fibre noise cancellation (FNC) setup) and the optical-fibre network between the lab and the remote location, as can be viewed in figure 2.1 and figure 3.1. An ultra-stable $\approx$ 1 Hz linewidth laser (Hz-laser) at 1550 nm wavelength is used both as an interrogator source to the optical fibre (coupling with acoustic disturbance) and the reference source. The laser output is split into a 90:10 ratio; the 10% light propagates through a 1 m fibre and is used as the nearly unperturbed frequency reference. The 90% light passes through the whole length of the fibre network, through AOM 1 to the remote site and again returning to the lab through AOM 2. Both the AOMs are fibre coupled attached to the fibre network and operate at 20 MHz centre frequency with $\pm$ 1 MHz bandwidth.

The 90% light going through the AOM 1 is center-shifted by -20 MHz and goes to the remote site and then comes back to the lab through AOM 2, where it is again center-shifted by -20 MHz and a beat-note of 40 MHz is formed at the coupler 4 (Cpl. 4) with the 10% reference source and is passed to the photodiode (PD) 2 t through the isolator (Iso.) 2

(carrying the out-of-loop information). At Cpl. 3, the Faraday-mirror (FM) 3 is placed to reflect the incoming light through the whole optical-fiber path again, thus again getting center-shifted twice at AOM 2 and AOM 1 respectively. Therefore, at Cpl. 1, we get a beat-note of 80 MHz between the laser light reflected from FM 1 (the reference) and centre-shifted laser coming back through the fibre, which is then passed to PD 1 through Iso. 1 (carrying in-loop information). Optical isolators Iso. 1 and Iso. 2 suppress unwanted reflection of photons, reducing the possibility of forming any unwanted optical resonator in the optical-fibre network.

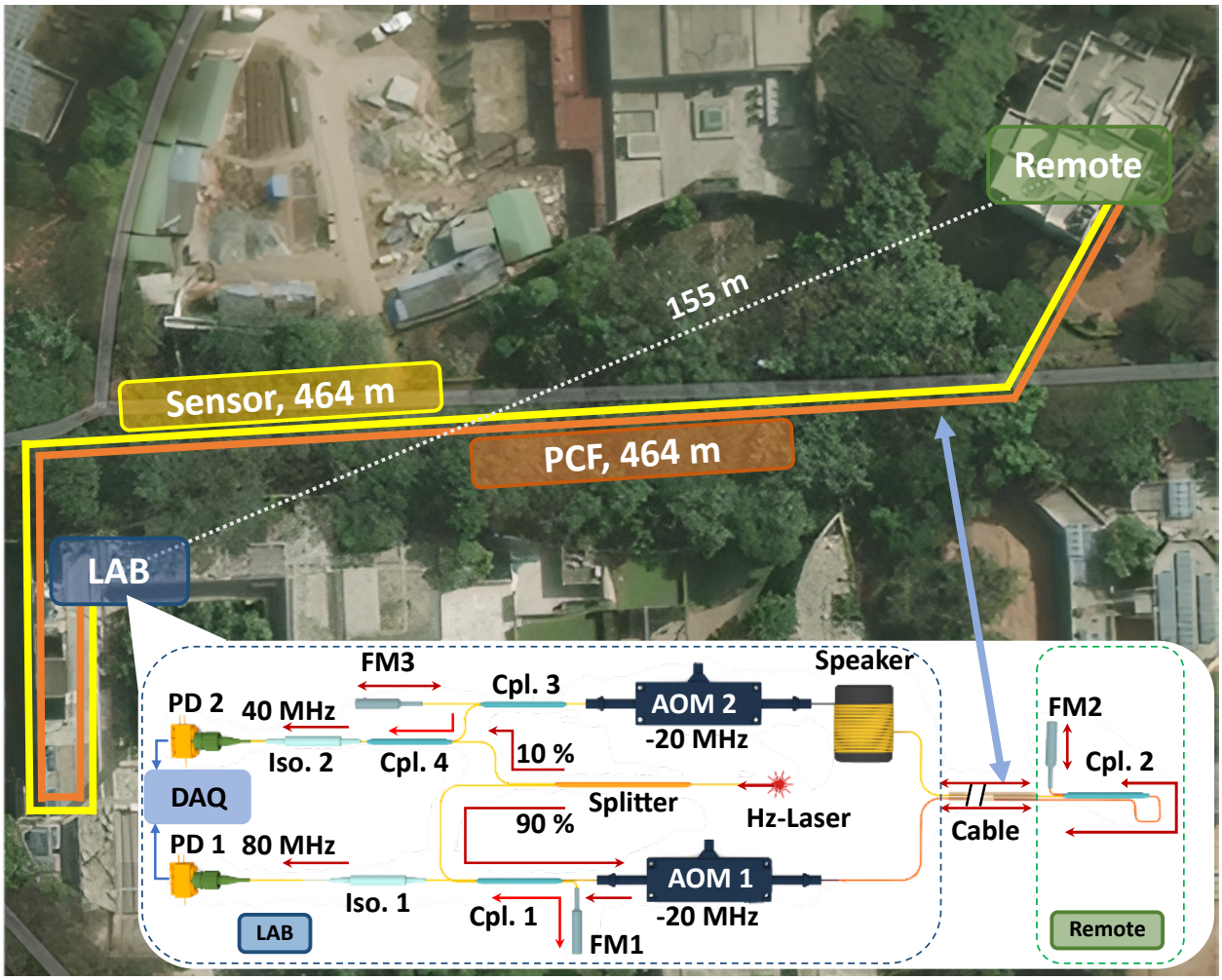

Figure 3.1: Experimental setup: Showing the components and optical-fiber network. Here Iso.: Isolator, Cpl.: Coupler, FM: Faraday Mirror, PD: Photodiode, AOM: Acousto-optic modulator.

The two beat notes detected by the photodiodes are converted to an electrical signal and

recorded by a data-acquisition system (DAQ). For our experiment, we used two instruments to record the data. One is an oscilloscope, which can provide us with short-term high-resolution dense time-series data, and another one is a precision frequency counter (K+K counter), which can provide us with long term data with a limitation of sampling frequency maximum upto 1 kHz.

3.2 Data Processing

We depict the data processing algorithm through a flowchart in figure 3.2.

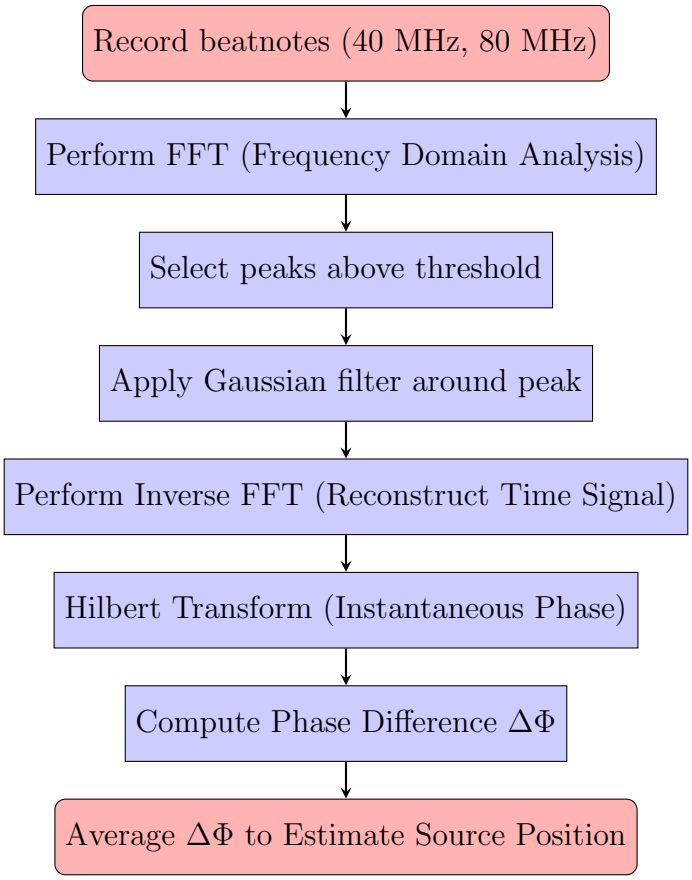

Figure 3.2: Flow chart showing the data processing algorithm.

We record two beat notes, one around 40 MHz and another around 80 MHz, using the photodiodes at the lab and a precision frequency counter (K+K counter) at a sampling rate

of 1000 Hz, as can be shown in figure 3.3.

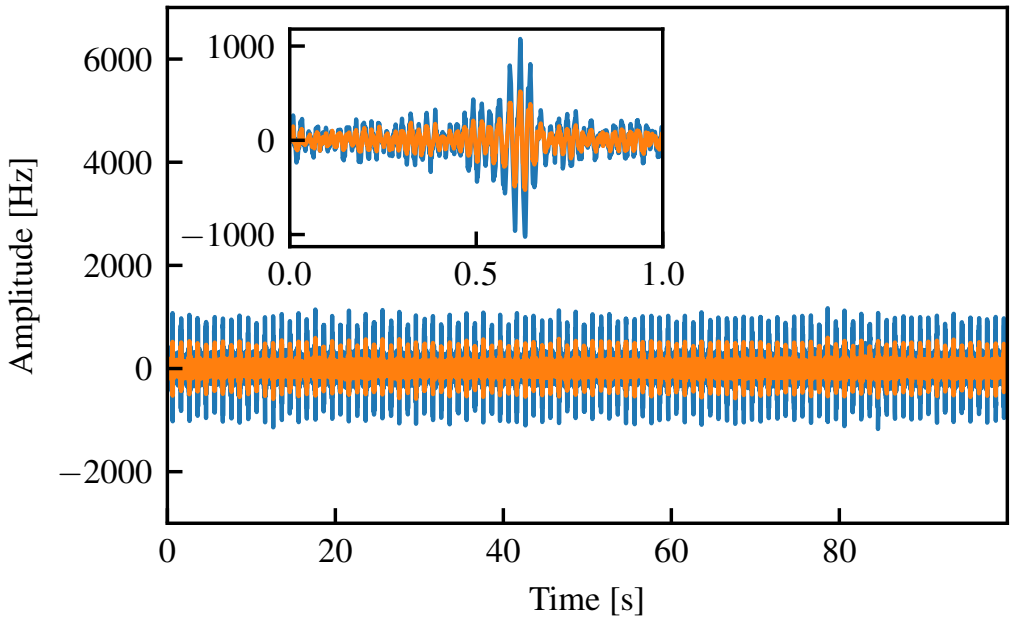

Figure 3.3: Recorded data (the centre frequency 40 MHz and 80 MHz are subtracted).

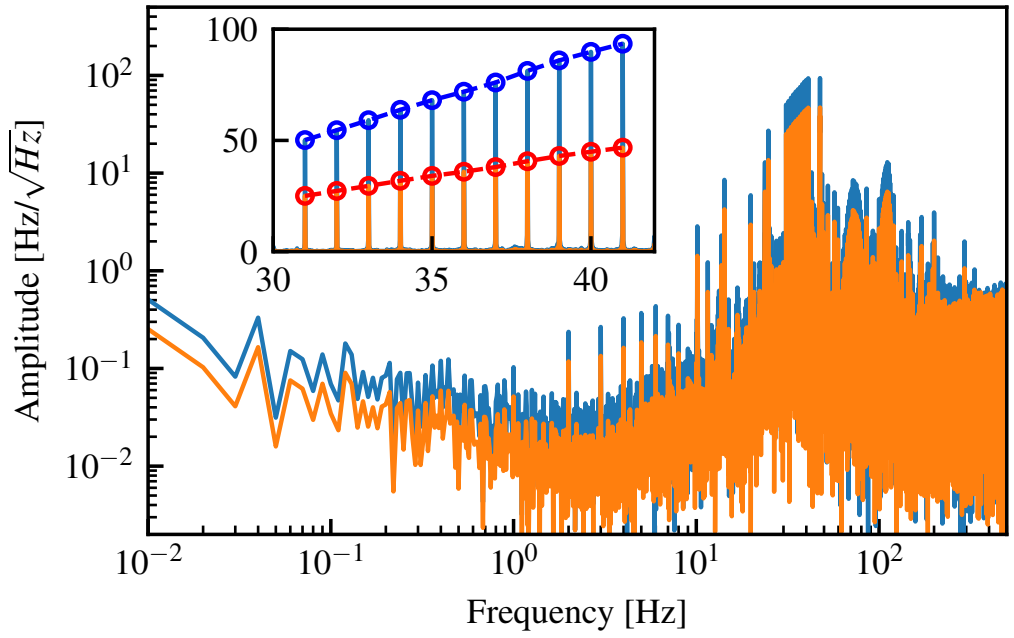

Figure 3.4: The frequency domain visualization of the recorded data.

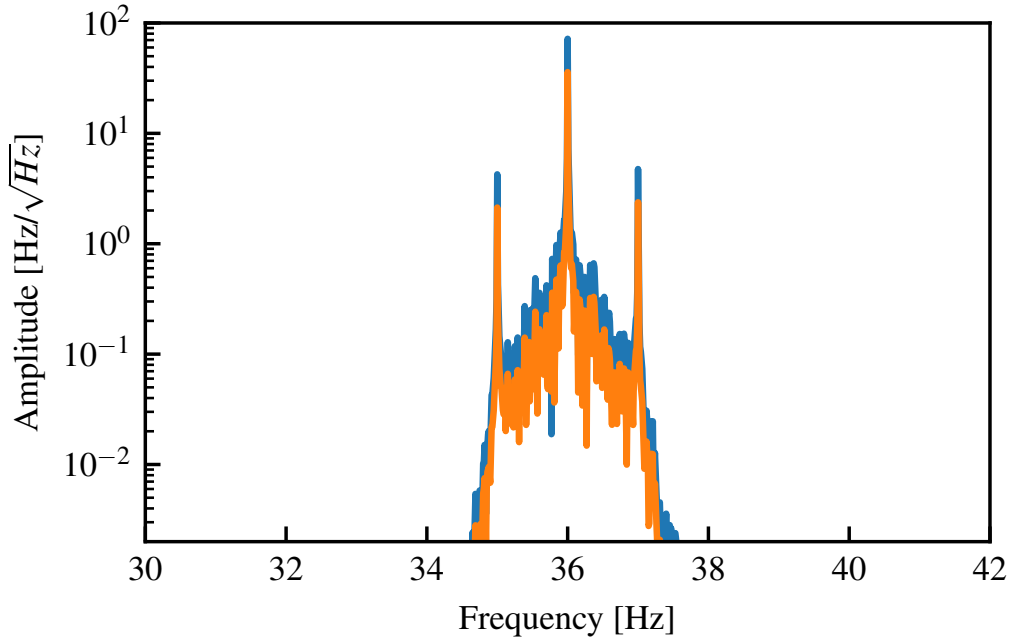

Figure 3.5: The Gaussian filtered FFT around 36 Hz.

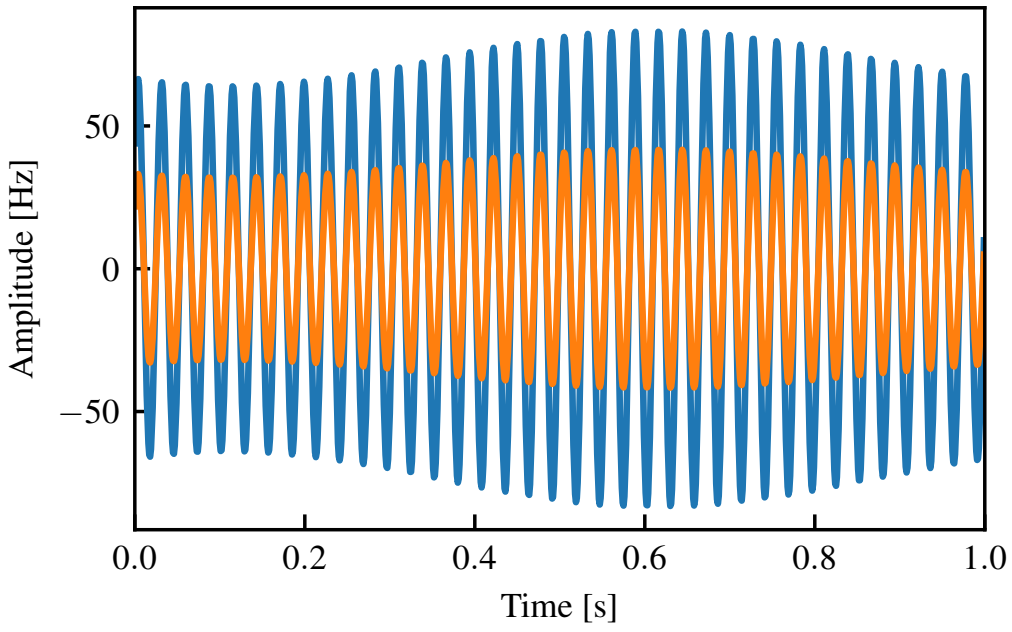

Figure 3.6: Reconstructed 36 Hz disturbance in time domain.

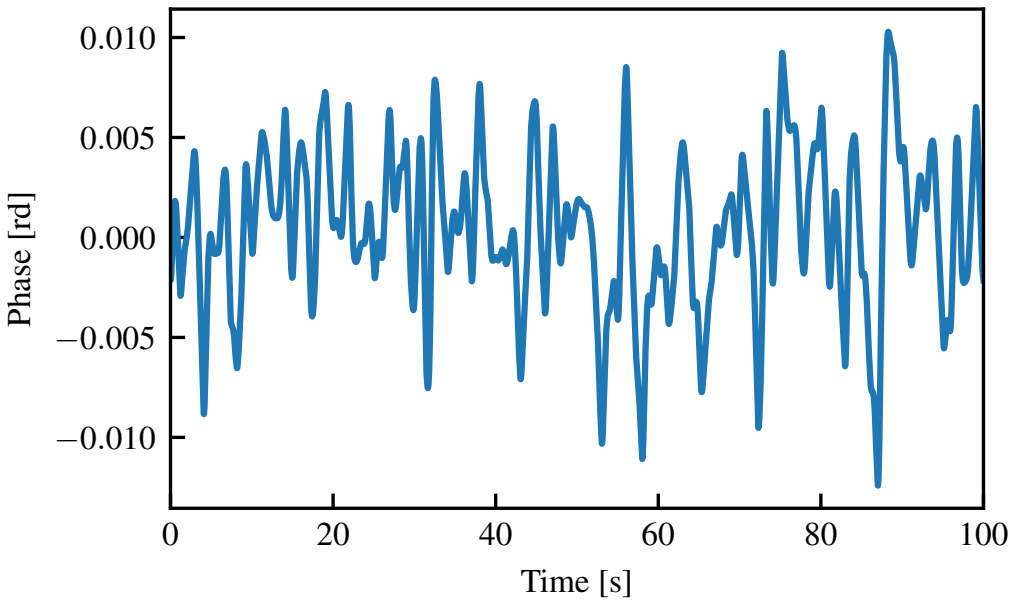

Figure 3.7: The phase-difference captured in the time domain.

We perform a fast Fourier transform (FFT) for both the time series (figure 3.3) and get the frequency domain information as shown in figure 3.4. We then select peaks above a certain threshold (amplitude value [Hz]) as shown in the inset of figure 3.4. Then, we put a Gaussian filter around one of the peaks for both the FFT data as shown in figure 3.5. Then, we perform an inverse Fourier transform (IFFT) and get the real part to reconstruct the acoustic source characteristics over time, as shown in figure 3.6. Finally, a Hilbert transform of the data gives us the instantaneous phase information, and a difference between them is shown in figure 3.7, which is our desired $\Delta\Phi$ monitored over time. Finally, we take an average value of the phase difference array and use it to find the position of the source according to equation 2.9. All data processing is performed using Python with the help of the following libraries: NumPy [55], SciPy [56], Pandas [57], and Matplotlib [58].

For the purpose of validation that we can locate and obtain the strength of an acoustic source, we have used a speaker (Bluetooth speaker as shown in the figure 3.1, with fibre wrapped around it), which acts as a frequency source capable of generating frequencies from 20 Hz to 20000 Hz and we have coiled optical fibre around it and kept it in the lab at a known position. To obtain the strength of the source, we used an accelerometer to validate our results.

Chapter 4

Simulations

4.1 Laser Stability & Laser Drift

The primary purpose of simulating an ultra-stable laser is to check what would happen if we used unstable lasers in the market with a broad linewidth. In figure 4.1a, we have simulated five lasers that have no drift in the centre frequency over time but differ in their linewidth and the fractional overlapping deviation (considering a 1550 nm laser) shows the stability of the laser frequency over time. This simulation gives us an idea of how much the position-localization error depends on the stability alone. The plot in orange (figure 4.1b) represents the laser we used in our experiment. Figure 4.1b shows the position resolution we can achieve using various laser stabilities. The plot in magenta in figure 4.1b is an experimentally derived result that shows how well our data matches the simulation.

Next, we simulate an ultra-stable laser with various drift rates to check the dependence of laser drift on position resolution for our experiment. In figure 4.2a, the blue plot shows the fractional overlapping deviation for an ultra-stable laser with no drift in the centre frequency. The orange plot represents a drift of 1 mHz/s, followed by green with a drift of 10 mHz/s, then red with drift 30 mHz/s, purple with drift 100 mHz/s and finally brown with drift 1000 mHz/s. A drift rate of 30 mHz/s represents the drift similar to the laser used in our experiment. Figure 4.2b shows that all the simulated results overlap, showing that the position resolution is independent of constant laser drift. The plot in magenta again shows the data corresponding to our experimental result.

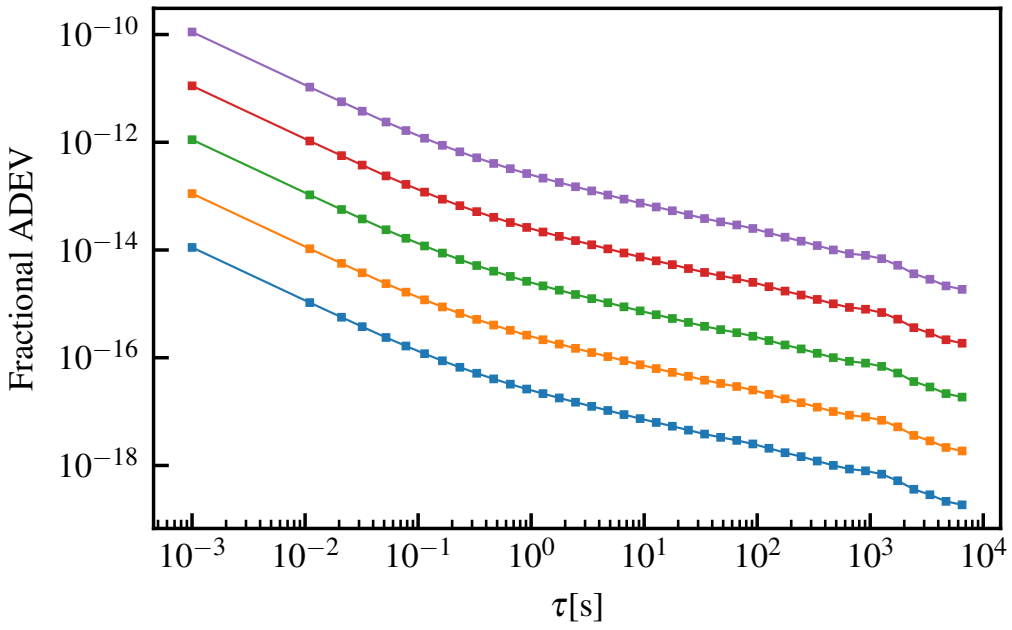

(a)

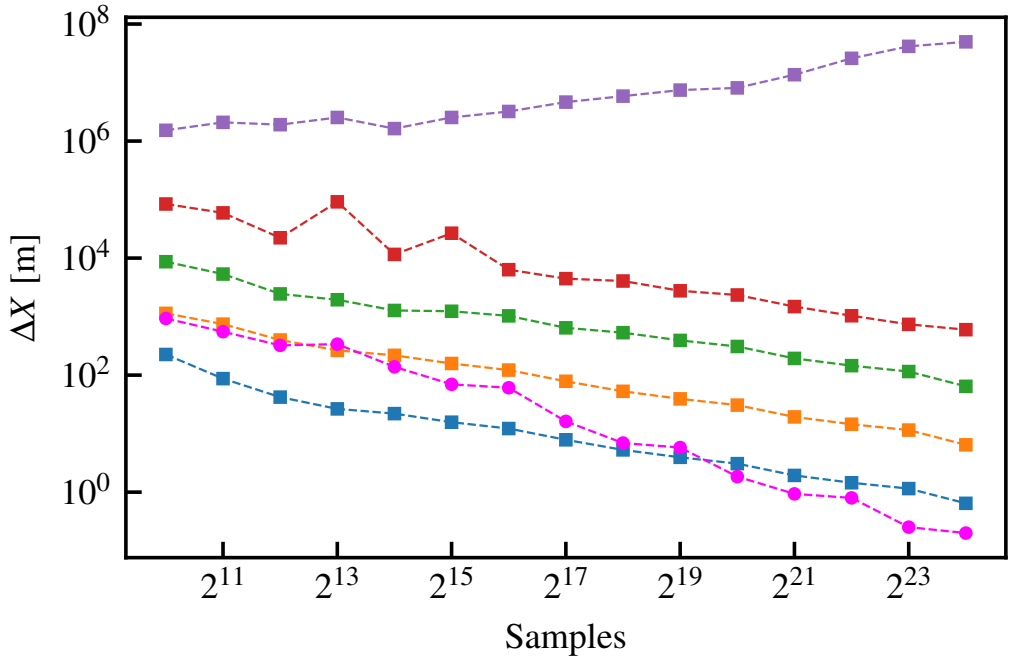

(b)

Figure 4.1: Simulating laser instability (a) and the various positions resolutions achieved using them (b).

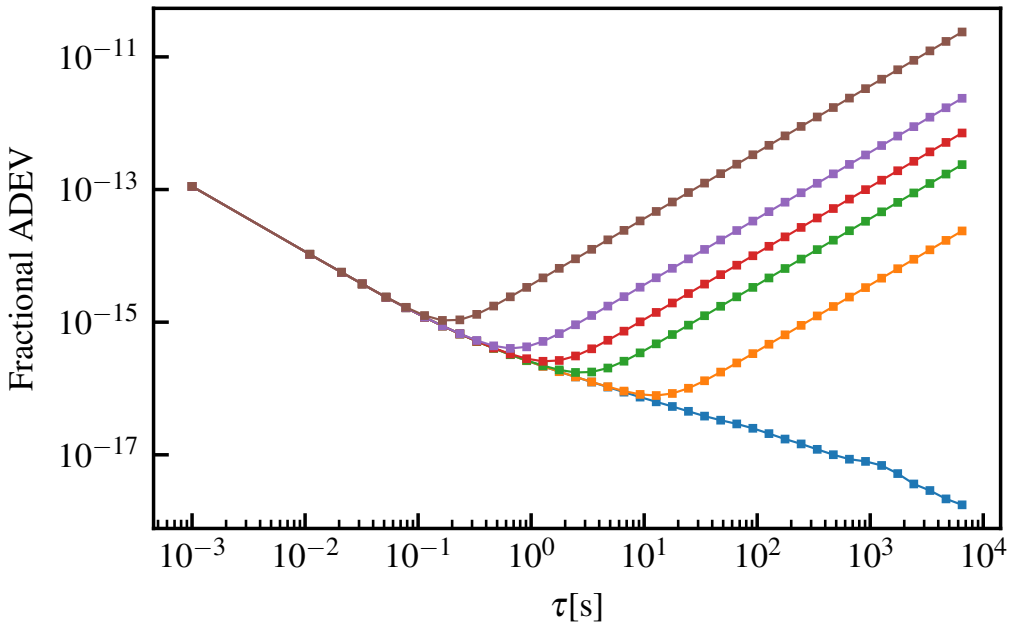

(a)

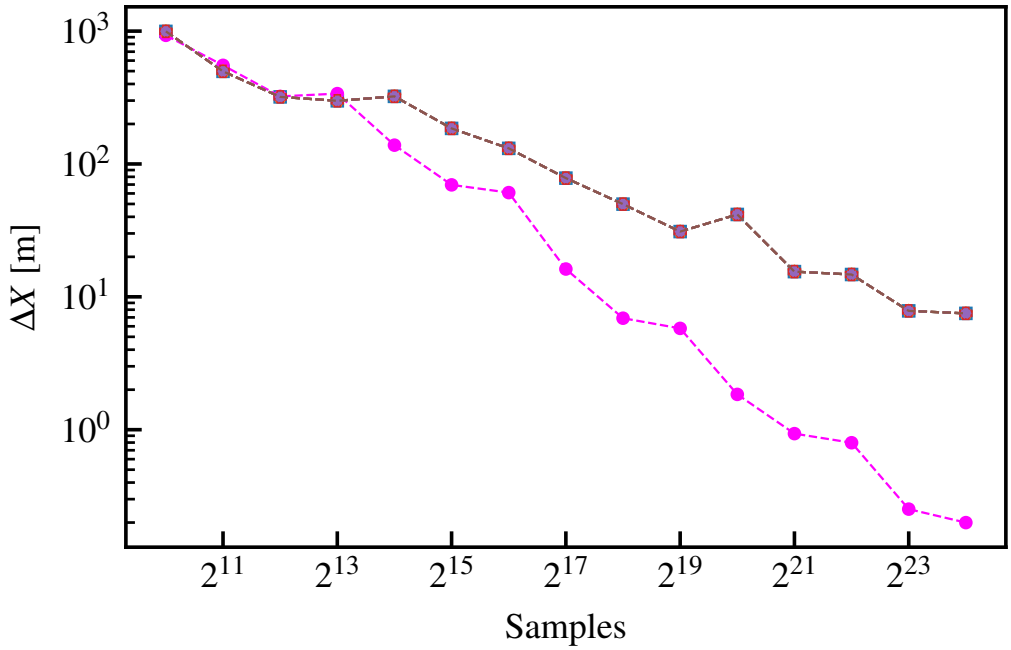

(b)

Figure 4.2: Simulating laser drift (a) and the various positions resolutions achieved using them (b).

4.2 Source strength

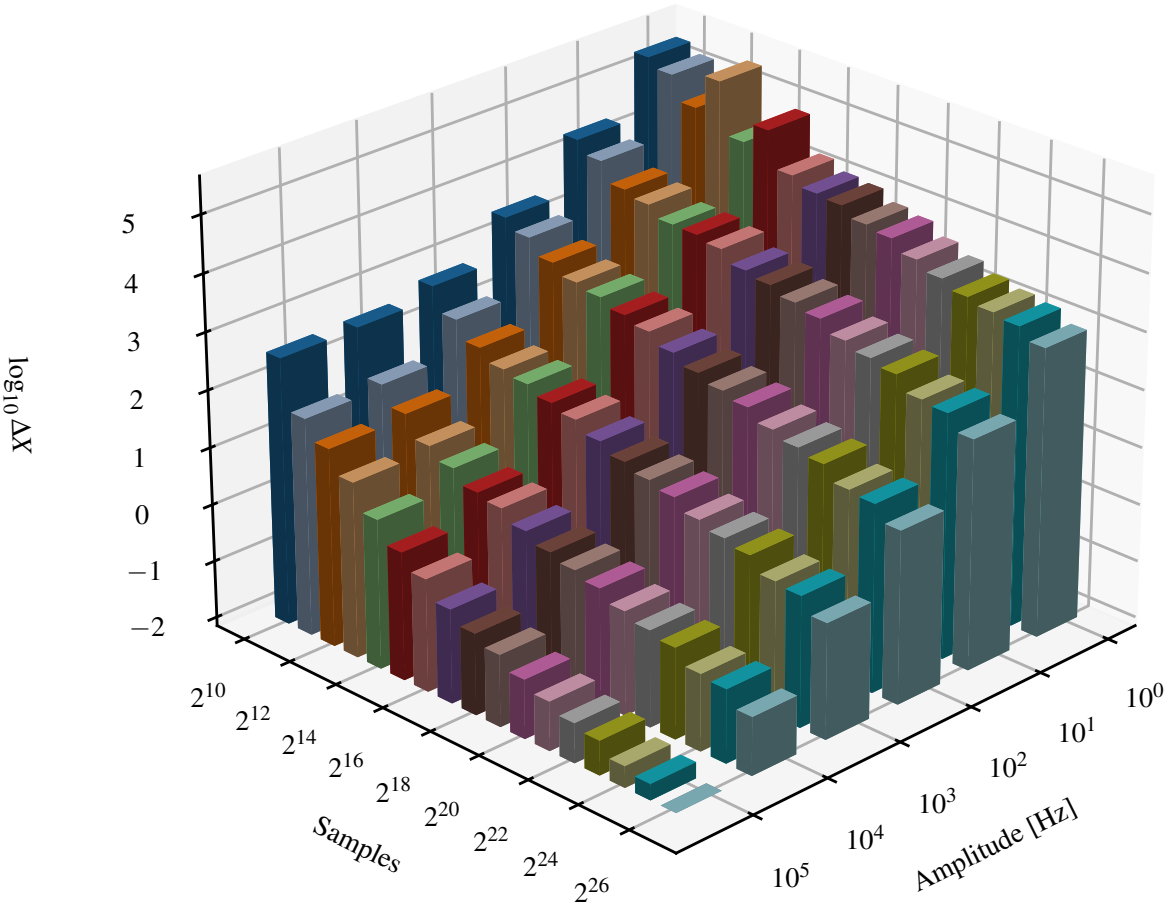

Figure 4.3: Position resolution corresponding to various source strengths.

Here, we are simulating various acoustic source strengths and trying to get an estimate of how fast we can localize the source. In figure 4.3, we simulate source strengths that are capable of producing frequency offset/excursion of 1 Hz, 10 Hz, 100 Hz, 1 kHz, 10 kHz and 100 kHz to the core laser frequency and see their position localization over time/number of samples. The simulation shows that strong sources can be localized faster with higher accuracy.

Thus, the three simulations highlight the various characteristics of the laser and the source that can affect the position localization process. These simulations also ensure that an ultra-stable laser is necessary for performing DAS with core laser signal.

Chapter 5

Results

5.1 Monitoring Frequency Over Time

As discussed in chapter 3, performing an FFT analysis gives us the frequency components. As we increase the number of samples used for calculating the FFT, the spectral resolution in the frequency domain improves. This is depicted in figure 5.1, where with an increasing number of samples, the frequency of 36 Hz produced by the speaker gets resolved. We find that the frequency produced by the speaker has an uncertainty in the milli-hertz (mHz) region as it is viewed that the measurement error saturates at approximately 1 mHz when we program the speaker to produce 36 Hz, shown as blue dots in figure 5.1.

We added a 36 Hz frequency numerically to background laser data when the speaker was turned off, once with monochromatic frequency (shown in connected red circles in figure 5.1) and another time with 36 Hz having mHz uncertainty (shown in connected blue circles in figure 5.1). This result suggests our system can accurately resolve an acoustic source's frequency. Also, we find that the signal-to-noise ratio improves as we increase the number of samples to resolve the frequency, shown for speaker produced 36 Hz (in green dots) and numerical added 36 Hz (shown as connected green boxes) in figure 5.1.

Thus, if we can resolve the frequency of an acoustic source, we can also monitor the frequencies interacting with the fibre over time. This can be done by taking a small portion of the data, performing FFT on it, and stacking them over time to get a spectrogram, as

shown in figure 5.2. We look at 100 s and perform the FFT. We get a frequency resolution of 0.01 Hz in the frequency axis. So two frequencies can be resolved if they differ by >= 0.01 Hz. Thus, if we make a tradeoff between frequency resolution and time resolution, we can monitor different frequency sources over time, as shown in the spectrogram (water-fall diagram) in figure 5.2. Here, the 11 horizontal lines from 31 Hz to 41 Hz are acoustic frequencies we give to the system using a speaker.

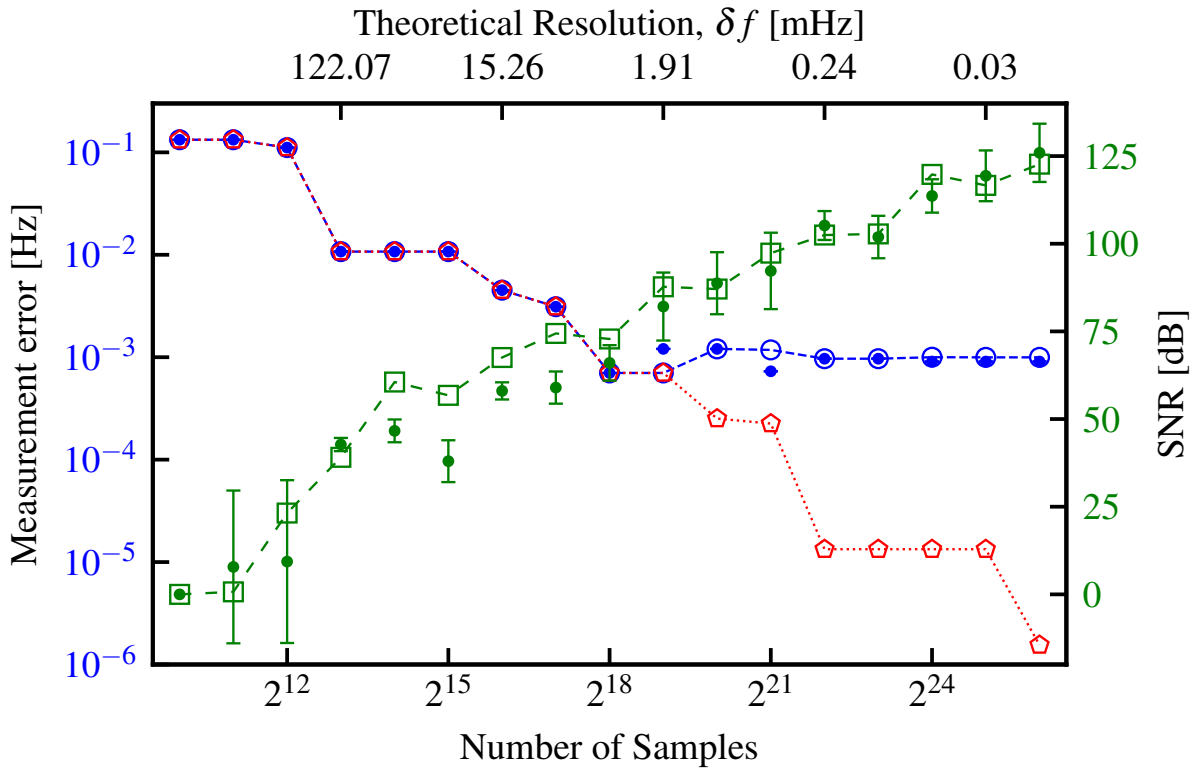

Figure 5.1: Frequency resolution of an acoustic source.

The Spectrogram in figure 5.2 shows frequencies monitored over one day while the frequencies produced by the speaker were turned on. The spectrograms in figure 5.3 and figure 5.4 show all the frequencies interacting with the optical fibre over 24 hours on two different days.

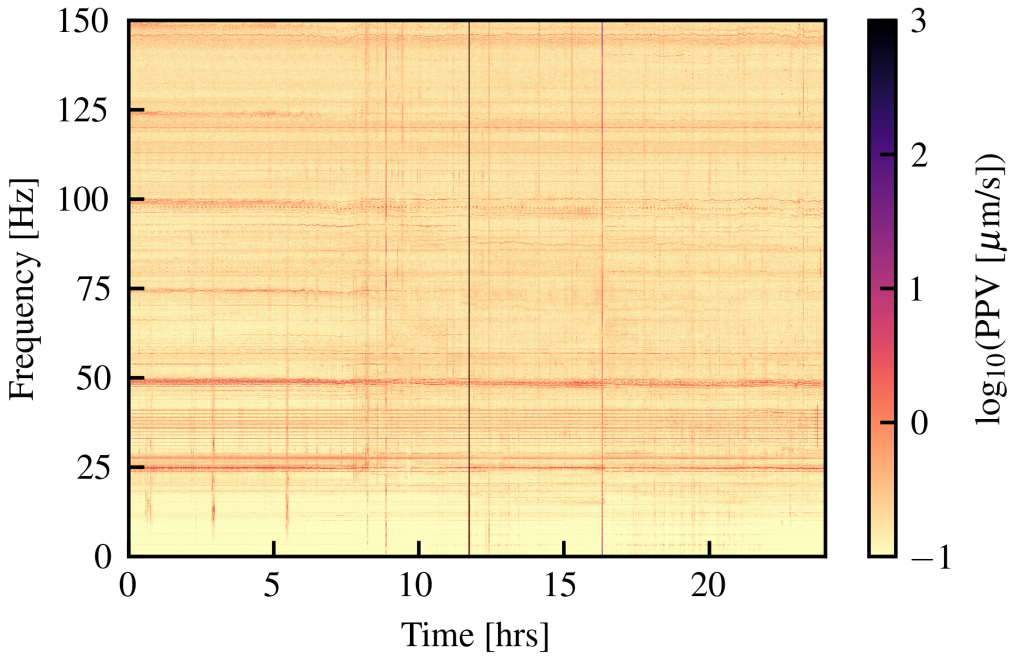

Figure 5.2: Spectrogram: Monitoring interacting frequency sources over time.

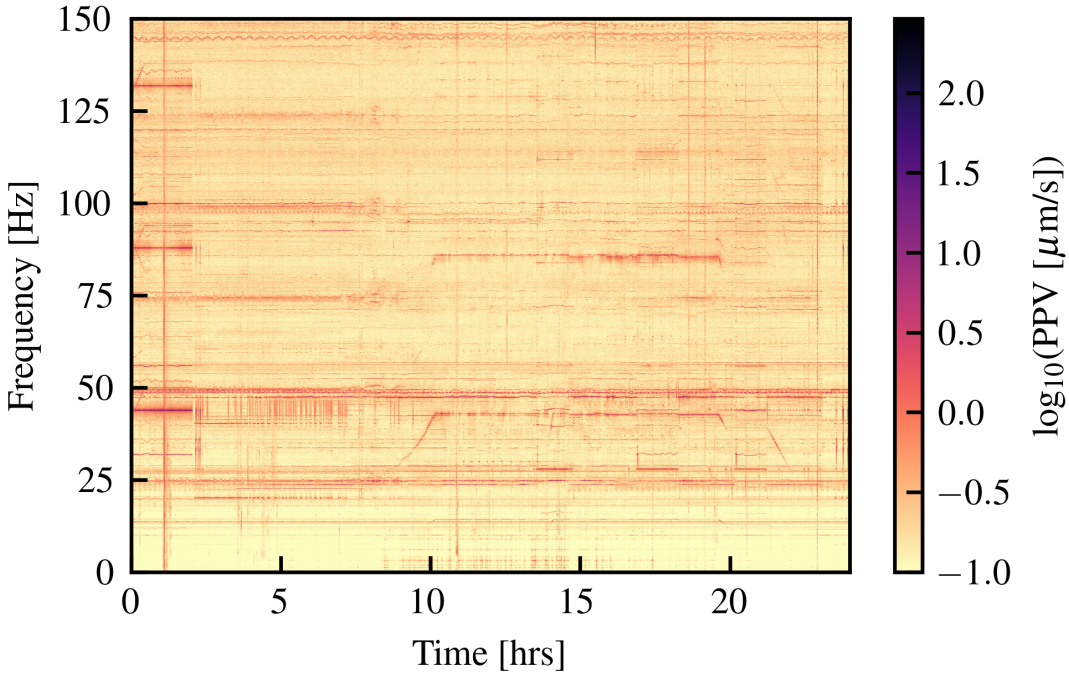

Figure 5.3: 24 Hrs spectrogram (speaker turned-off) on September 7, 2024.

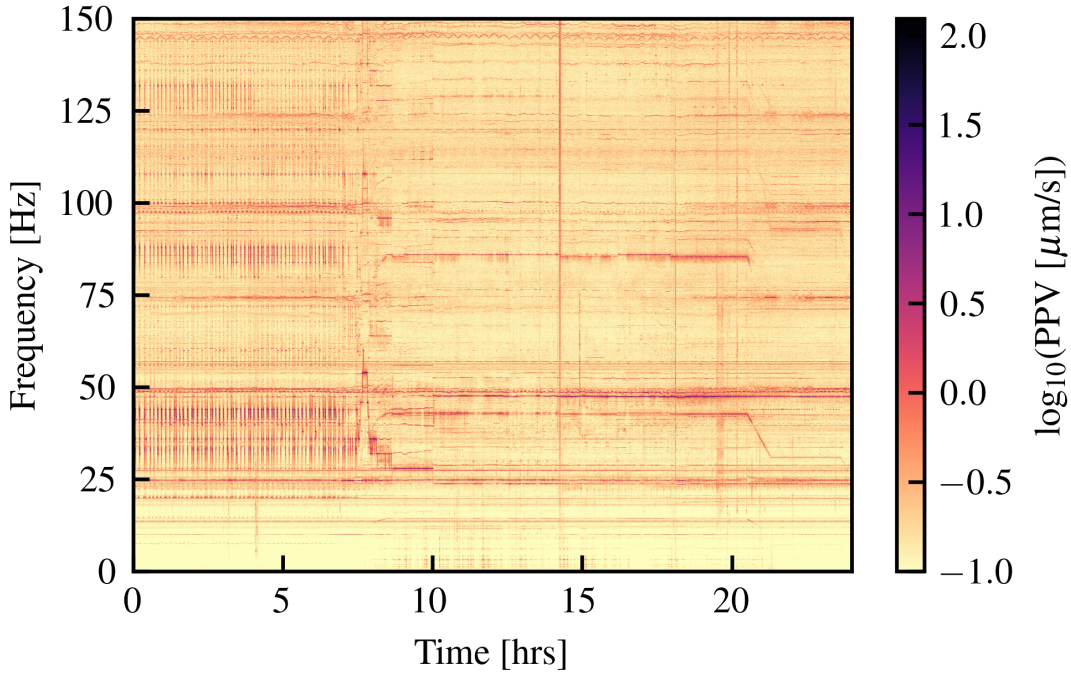

Figure 5.4: 24 Hrs spectrogram (speaker turned-off) on September 8, 2024.

5.2 Estimating the strength of a disturbance

From the FFT analysis, we can find the corresponding frequency excursion from the centre frequency of the 40 MHz beat note caused by an acoustic source. This excursion can give us an estimate of the strength of the source. This amplitude excursion directly corresponds to the strain change caused, which in turn can give us the length change of the fibre. The length change can be correlated to the displacement of the particles near the optical fibre, which can be translated to their velocities and is termed peak-particle-velocity (PPV). We can thus calculate this value and validate it using an accelerometer as shown in figure 5.5a. This leads us to find the noise floor for our DAS system over the currently deployed fibre, which is given in figure 5.5. The noise-floor plot suggests that our system is sensitive to the nm/s level of PPV values in the low-frequency regions. This is an important indication showing that we can detect faint micro-seismic vibrations using our system.

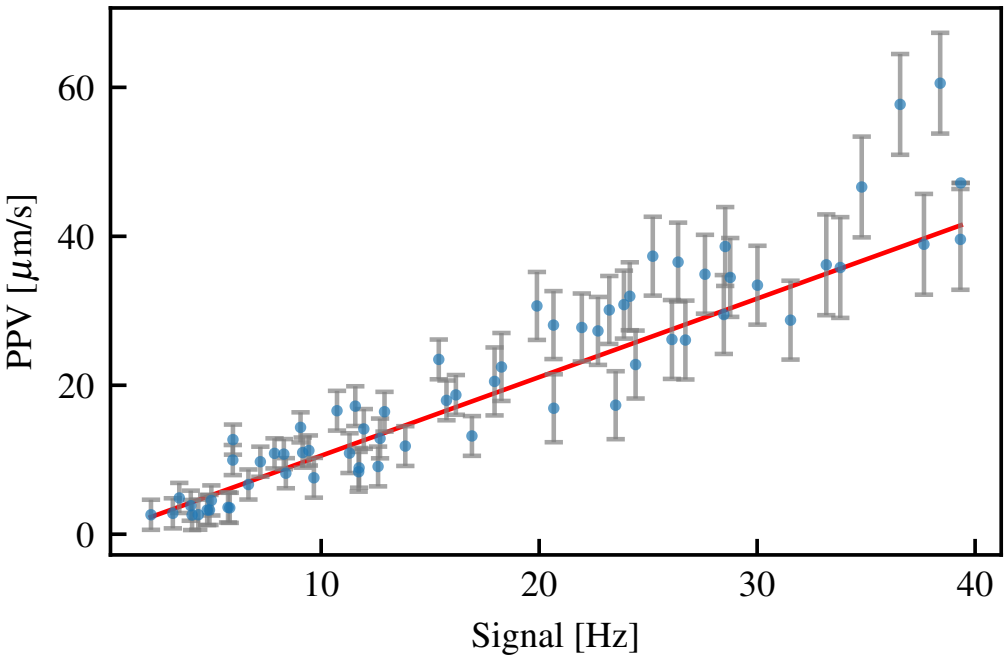

(a)

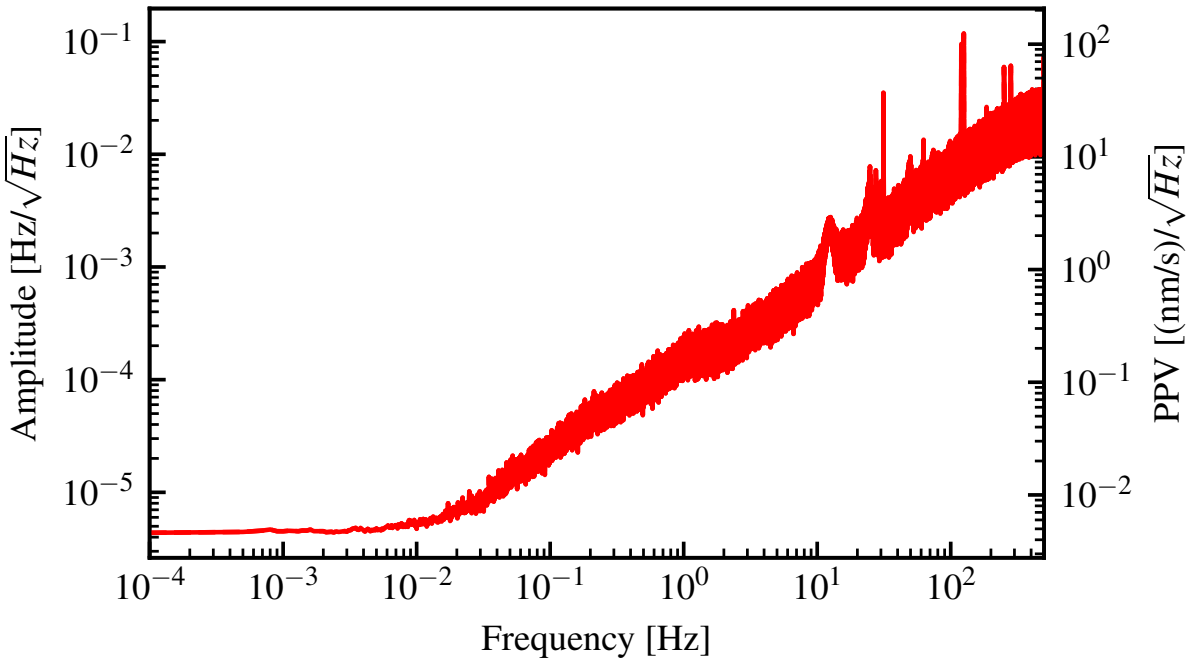

(b)

Figure 5.5: (a) Frequency excursion (amplitude [Hz]) produced by an acoustic source and the calculated PPV value from it (in red), and the measured values (in blue dots) using an accelerometer. (b) Noise floor for the deployed fiber-optic network.

5.3 Locating a disturbance

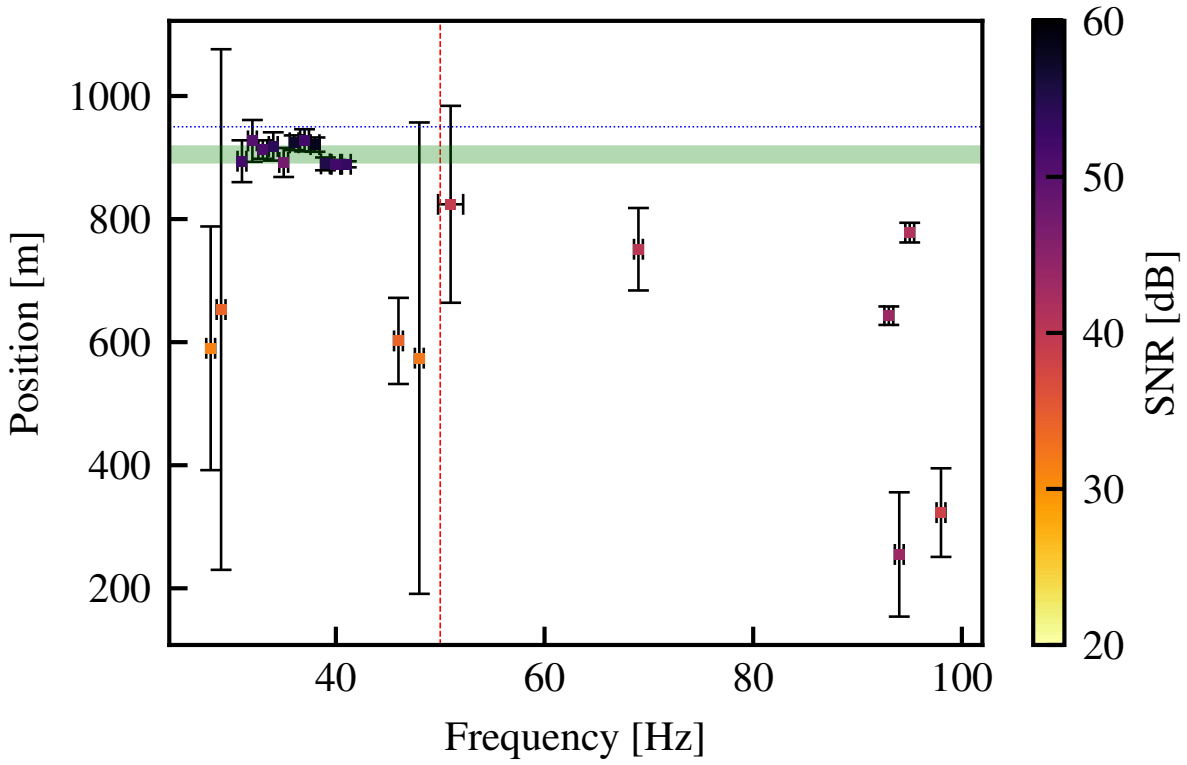

Figure 5.6: Acoustic source frequencies and their positions.

We can detect the frequencies the speaker produces with the best accuracy of $\pm 5\,\mathrm{m}$ and an average accuracy of $\pm(10-14)\,\mathrm{m}$. This is depicted in figure 5.6, where the frequencies produced by the speaker are present in the light green band (31 to 41 Hz), and a few of the other frequency sources are also shown. The error bars do not show the position accuracy. Rather, they represent the interaction length with the optical fibre. Multiple chunks of 2^{21} samples were processed to find the locations for a particular frequency, and the mean positions were collected. The error bars show the shift in the mean position, which tells us that the frequency source is not localized at a single point along the fibre but interacts with the optical fibre over a certain interaction length.

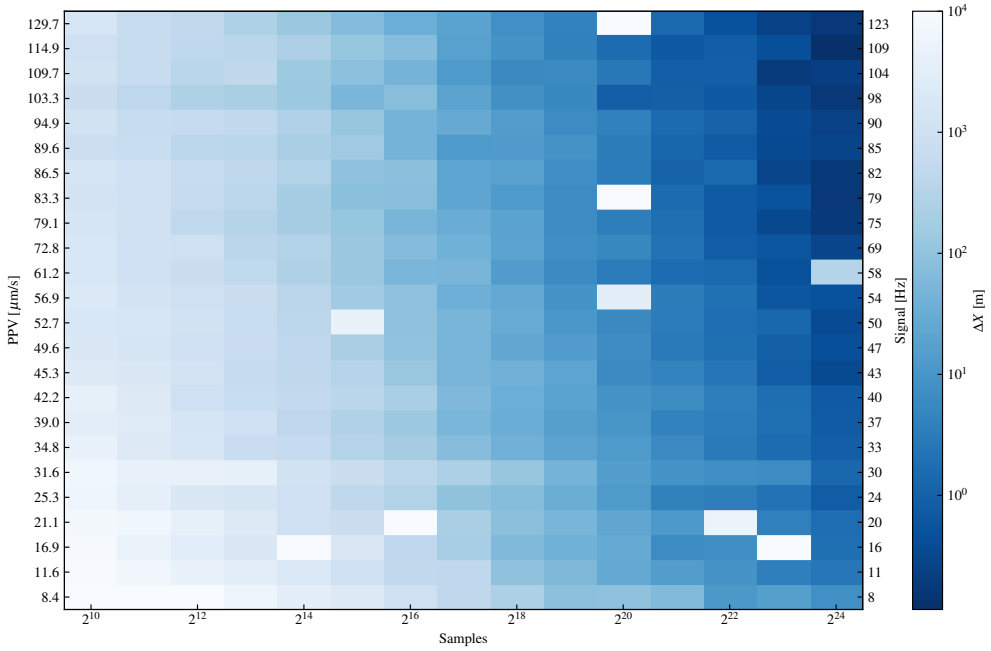

Figure 5.7: Position resolution over the number of samples and the strength of the acoustic source. Acoustic source: Frequencies produced by the speaker.

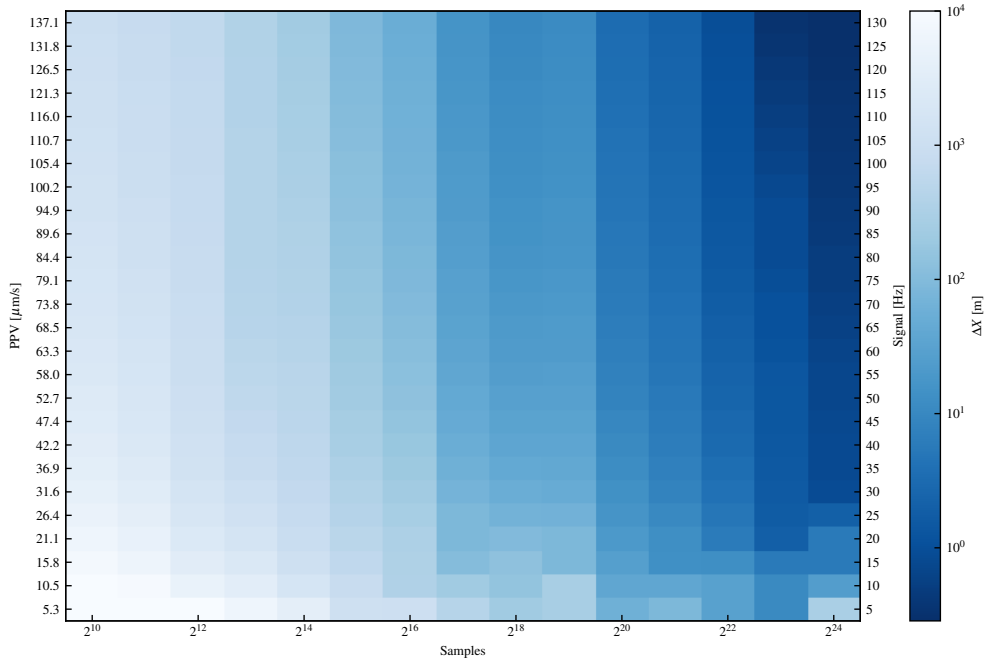

Figure 5.8: Position resolution over the number of samples and the strength of the acoustic source. Acoustic source: A numerically simulated monochromatic source was added to the background data and localized at a single point.

The frequencies produced by the speaker are localized over an interaction length of 5 m coil wrapped around the speaker. We then try to estimate the number of samples required to localize a source to the strength of the acoustic source. This can be visualized in the figure 5.7.

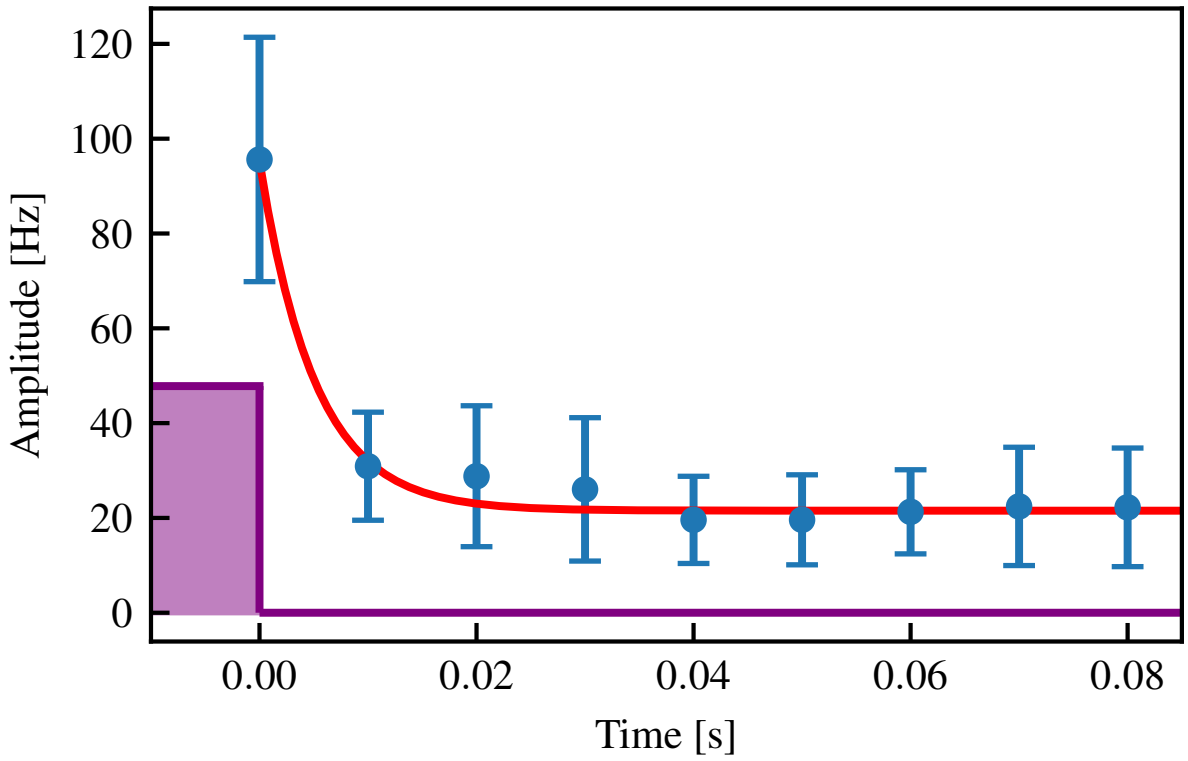

Figure 5.9: Decay of a 150 Hz pulsed acoustic source. The area in purple shows the end of a pulse, and the red line shows the fitted decay of the pulse with τ=0.5 ms.

Among the various sources for position accuracy, we can consider that the decay of acoustic source strength along the length of the fibre material can lead to position inaccuracy even when the source is localized to a single point. This can be confirmed by the plot 5.9, which shows the amplitude decay of a 150 Hz acoustic pulsed source. The decay time constant of $\tau = 0.5$ ms corresponds to a travel length of 1 m from the source by an acoustic disturbance while decaying to 1/e of the original strength.

Chapter 6

Conclusion

The research presented in this thesis has demonstrated the ability to monitor the frequency of an acoustic source interacting with optical fibres. By leveraging an ultra-stable laser-based distributed acoustic sensing system (*ul*DAS), we have achieved remarkable sensitivity in detecting even the weakest vibrations and accurately locating their sources. Our system exhibits a position resolution that competes with some of the most advanced instruments used in industry and laboratory settings, as illustrated in Figure 6.1.

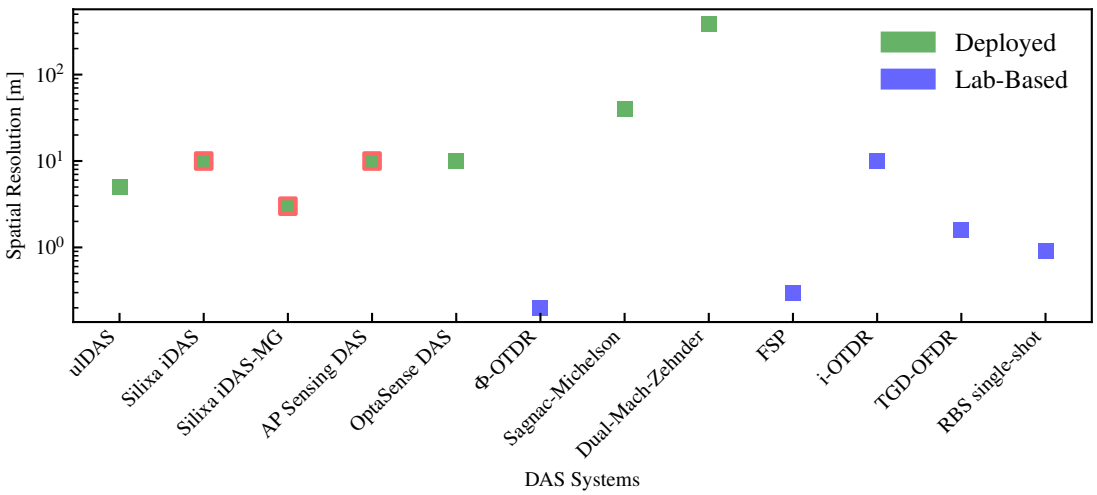

Figure 6.1: Position resolution of Our system (*ul*DAS) with various industry and lab-based instruments.

Beyond its immediate capabilities, *ul*DAS holds great promise as a calibration instrument for accelerometers, offering an unprecedented level of precision. One of its most critical applications lies in gravitational wave detection, where our system can contribute validation data to better understand and mitigate seismic and acoustic vibrations affecting interferometer arms. The ability to distinguish between environmental noise and true gravitational wave signals is crucial for enhancing the sensitivity of these detectors.

Moreover, the distributed nature of *ul*DAS introduces a wide array of applications:

- **Early Warning Systems**: By continuously monitoring seismic noise, our system can provide early warnings for natural calamities such as earthquakes, tsunamis, and volcanic eruptions. Differentiating abnormal seismic activity from background noise can significantly improve disaster preparedness and response.
- **Surveillance and Strategic Navigation**: Underground and deep-sea seismic monitoring are traditionally outside the reach of satellite-based imaging. Our system can provide critical insights into seismic activity in these inaccessible regions, offering a reliable alternative to satellite-dependent navigation—particularly in situations where satellite signals might be jammed or unavailable.
- **Structural Health Monitoring**: The ability to detect minute vibrations and structural instabilities makes *ul*DAS an invaluable tool for monitoring infrastructure such as bridges, flyovers, and railway tracks. Early detection of cracks and weaknesses can prevent catastrophic failures, ensuring public safety.
- **Geological Data Collection and AI Integration**: The fibre-based distributed sensors can continuously monitor seismic vibrations and temperature variations over extended periods and large geographic areas. This extensive data collection can contribute to geological research and be leveraged for AI and machine learning applications to enhance predictive models and automated analysis [59].

The potential of *ul*DAS extends far beyond the laboratory. Its integration into real-world applications could revolutionize fields ranging from disaster prevention to space exploration. The foundation laid in this work paves the way for further advancements in distributed acoustic sensing, ensuring that this technology continues to evolve and address some of the most pressing scientific and societal challenges of our time.

Bibliography

[1] Z. Fang, K. K. Chin, R. Qu, and H. Cai, *Fundamentals of Optical Fiber Sensors*. Hoboken, NJ: John Wiley & Sons, Inc., 2012, ISBN: 9780470575406. DOI: 10.1002/9781118381717. [Online]. Available: https://doi.org/10.1002/9781118381717.

[2] P. Kuznetsov, D. Sudas, and E. Savelyev, "Fiber optic lossy mode resonance based sensor for aggressive liquids," *Sensors and Actuators A: Physical*, vol. 321, p. 112 576, 2021, ISSN: 0924-4247. DOI: https://doi.org/10.1016/j.sna.2021.112576. [Online]. Available: https://www.sciencedirect.com/science/article/pii/S0924424721000376.

[3] D.-K. Zhang, P. C. Hills, C. Zheng, T. F. Wall, and P. Samson, "Fibre optic ignition of combustible gas mixtures by the radiative heating of small particles," *Symposium (International) on Combustion*, vol. 24, no. 1, pp. 1761–1767, 1992, Twenty-Fourth Symposium on Combustion, ISSN: 0082-0784. DOI: https://doi.org/10.1016/S0082-0784(06)80206-7. [Online]. Available: https://www.sciencedirect.com/science/article/pii/S0082078406802067.

[4] A. H. Hartog, *An Introduction to Distributed Optical Fibre Sensors*, 1st. Boca Raton: CRC Press, 2017, p. 472, ISBN: 9781315119014. DOI: 10.1201/9781315119014. [Online]. Available: https://doi.org/10.1201/9781315119014.

[5] A. Barrias, J. R. Casas, and S. Villalba, "A review of distributed optical fiber sensors for civil engineering applications," *Sensors*, vol. 16, no. 5, 2016, ISSN: 1424-8220. DOI: 10.3390/s16050748. [Online]. Available: https://www.mdpi.com/1424-8220/16/5/748.

[6] P. Healey, "Instrumentation principles for optical time domain reflectometry," *Journal of Physics E: Scientific Instruments*, vol. 19, no. 5, p. 334, May 1986. DOI: 10.1088/

0022-3735/19/5/002. [Online]. Available: https://dx.doi.org/10.1088/0022-3735/19/5/002.

[7] C. A. Lopez-Mercado, D. A. Korobko, I. O. Zolotovskii, and A. A. Fotiadi, "Application of dual-frequency self-injection locked dfb laser for brillouin optical time domain analysis," *Sensors*, vol. 21, no. 20, 2021, ISSN: 1424-8220. DOI: 10.3390/s21206859. [Online]. Available: https://www.mdpi.com/1424-8220/21/20/6859.

[8] J. Dakin, D. Pratt, G. Bibby, and J. Ross, "Distributed optical fibre raman temperature sensor using a semiconductor light source and detector," *Electronics Letters*, vol. 21, pp. 569–570, 13 1985. DOI: 10.1049/el:19850402. eprint: https://digital-library.theiet.org/doi/pdf/10.1049/el%3A19850402. [Online]. Available: https://digital-library.theiet.org/doi/abs/10.1049/el%3A19850402.

[9] A. G. Kuznetsov, S. A. Babin, and I. S. Shelemba, "Fibreoptic distributed temperature sensor with spectral filtration by directional fibre couplers," *Quantum Electronics*, vol. 39, no. 11, p. 1078, Nov. 2009. DOI: 10.1070/QE2009v039n11ABEH014173. [Online]. Available: https://dx.doi.org/10.1070/QE2009v039n11ABEH014173.

[10] Z. Liu and A. K. Kim, "Review of recent developments in fire detection technologies," *Journal of Fire Protection Engineering*, vol. 13, no. 2, pp. 129–151, 2003. DOI: 10.1177/1042391503013002003. eprint: https://journals.sagepub.com/doi/pdf/10.1177/1042391503013002003. [Online]. Available: https://journals.sagepub.com/doi/abs/10.1177/1042391503013002003.

[11] B. Gorshkov, G. Gorshkov, and K. Zhukov, "Distributed fibre-optic temperature sensor for cryogenic applications based on detection of boson components of raman light scattering," *Quantum Electronics*, vol. 50, no. 5, p. 506, May 2020. DOI: 10.1070/QEL17238. [Online]. Available: https://dx.doi.org/10.1070/QEL17238.

[12] M. G. Tanner, S. D. Dyer, B. Baek, R. H. Hadfield, and S. Woo Nam, "High-resolution single-mode fiber-optic distributed raman sensor for absolute temperature measurement using superconducting nanowire single-photon detectorsa)," *Applied Physics Letters*, vol. 99, no. 20, p. 201 110, Nov. 2011, ISSN: 0003-6951. DOI: 10.1063/1.3656702. eprint: https://pubs.aip.org/aip/apl/article-pdf/doi/10.1063/1.3656702/16738433/201110_1_online.pdf. [Online]. Available: https://doi.org/10.1063/1.3656702.

[13] Y. Liu, L. Ma, C. Yang, W. Tong, and Z. He, "Long-range raman distributed temperature sensor with high spatial and temperature resolution using graded-index few-mode fiber," *Opt. Express*, vol. 26, no. 16, pp. 20 562–20 571, Aug. 2018. DOI: 10.1364/OE.26.020562. [Online]. Available: https://opg.optica.org/oe/abstract.cfm?URI=oe-26-16-20562.

[14] A. Kuznetsov, D. Kharenko, S. Babin, I. Tsydenzhapov, and I. Shelemba, "Ultra-long fibre-optic distributed raman temperature sensor," *Quantum Electronics*, vol. 47, no. 10, p. 967, Nov. 2017. DOI: 10.1070/QEL16436. [Online]. Available: https://dx.doi.org/10.1070/QEL16436.

[15] J. Li *et al.*, "Temperature resolution improvement in raman-based fiber-optic distributed sensor using dynamic difference attenuation recognition," *Sensors*, vol. 20, no. 23, 2020, ISSN: 1424-8220. DOI: 10.3390/s20236922. [Online]. Available: https://www.mdpi.com/1424-8220/20/23/6922.

[16] C. Feng, J. E. Kadum, and T. Schneider, "The state-of-the-art of brillouin distributed fiber sensing," in *Fiber Optic Sensing*, S.-K. Liaw, Ed., Rijeka: IntechOpen, 2019, ch. 5. DOI: 10.5772/intechopen.84684. [Online]. Available: https://doi.org/10.5772/intechopen.84684.

[17] M. A. Taranov, B. G. Gorshkov, A. E. Alekseev, and V. T. Potapov, "Distributed strain and temperature sensing over 100 km using tunable-wavelength otdr based on mems filters," *Appl. Opt.*, vol. 60, no. 11, pp. 3049–3054, Apr. 2021. DOI: 10.1364/AO.419837. [Online]. Available: https://opg.optica.org/ao/abstract.cfm?URI=ao-60-11-3049.

[18] T. Galkovski, Y. Lemcherreq, J. Mata-Falcón, and W. Kaufmann, "Fundamental studies on the use of distributed fibre optical sensing on concrete and reinforcing bars," *Sensors*, vol. 21, no. 22, 2021, ISSN: 1424-8220. DOI: 10.3390/s21227643. [Online]. Available: https://www.mdpi.com/1424-8220/21/22/7643.

[19] T. Parker, S. Shatalin, and M. Farhadiroushan, "Distributed acoustic sensing - a new tool for seismic applications," *First Break*, vol. 32, no. 2, 2014. DOI: 10.3997/1365-2397.2013034. [Online]. Available: https://doi.org/10.3997/1365-2397.2013034.

[20] S. V. Shatalin, V. N. Treschikov, and A. J. Rogers, "Interferometric optical time-domain reflectometry for distributed optical-fiber sensing," *Appl. Opt.*, vol. 37, no. 24, pp. 5600–5604, Aug. 1998. DOI: 10.1364/AO.37.005600. [Online]. Available: https://opg.optica.org/ao/abstract.cfm?URI=ao-37-24-5600.

[21] L. D. van Putten, A. Masoudi, J. Snook, and G. Brambilla, "Numerical modelling of a distributed acoustic sensor based on ultra-low loss-enhanced backscattering fibers," *Sensors*, vol. 21, no. 20, 2021, ISSN: 1424-8220. DOI: 10.3390/s21206869. [Online]. Available: https://www.mdpi.com/1424-8220/21/20/6869.

[22] Y. Wang *et al.*, "Optical fiber vibration sensor using least mean square error algorithm," *Sensors*, vol. 20, no. 7, 2020, ISSN: 1424-8220. DOI: 10.3390/s20072000. [Online]. Available: https://www.mdpi.com/1424-8220/20/7/2000.

[23] X. He, M. Zhang, L. Gu, S. Xie, F. Liu, and H. Lu, "Performance improvement of dual-pulse heterodyne distributed acoustic sensor for sound detection," *Sensors*, vol. 20, no. 4, 2020, ISSN: 1424-8220. DOI: 10.3390/s20040999. [Online]. Available: https://www.mdpi.com/1424-8220/20/4/999.

[24] L. B. Liokumovich, N. A. Ushakov, O. I. Kotov, M. A. Bisyarin, and A. H. Hartog, "Fundamentals of optical fiber sensing schemes based on coherent optical time domain reflectometry: Signal model under static fiber conditions," *Journal of Lightwave Technology*, vol. 33, no. 17, pp. 3660–3671, 2015. DOI: 10.1109/JLT.2015.2449085.

[25] J. Rayleigh, *The Theory of Sound*. New York, NY, USA: Macmillan, 1896, vol. 2.

[26] J. Juarez, E. Maier, K. N. Choi, and H. Taylor, "Distributed fiber-optic intrusion sensor system," *Journal of Lightwave Technology*, vol. 23, no. 6, pp. 2081–2087, 2005. DOI: 10.1109/JLT.2005.849924.

[27] C. Madsen, T. Bae, and T. Snider, "Intruder signature analysis from a phase-sensitive distributed fiber-optic perimeter sensor," in *Proceedings of the Fiber Optic Sensors and Applications V 2007*, Boston, MA, USA, Sep. 2007, pp. 6770–19.

[28] X. Yu, D. Zhou, B. Lu, S. Liu, and M. Pan, "Phase-sensitive optical time domain reflectometer for distributed fence-perimeter intrusion detection," in *Fiber Optic Sensors and Applications XII*, vol. 9679, Bellingham, WA, USA: SPIE, 2015.

[29] I. White, M. Crisp, and R. Penty, "A photonics based intelligent airport surveillance and tracking system," in *Proceedings of the 2010 24th IEEE International Conference on Advanced Information Networking and Applications*, Perth, Australia, Apr. 2010, pp. 11–16.

[30] S. Merlo *et al.*, "Runways ground monitoring system by phase-sensitive optical-fiber otdr," in *Proceedings of the 2017 IEEE International Workshop on Metrology for AeroSpace (MetroAeroSpace)*, Padua, Italy, Jun. 2017, pp. 523–529.

[31] S. Shatalin, T. Parker, and M. Farhadiroushan, "High definition seismic and microseismic data acquisition using distributed and engineered fiber optic acoustic sensors," in *Distributed Acoustic Sensing in Geophysics*, Hoboken, NJ, USA: Wiley, 2021, pp. 1–32.

[32] M. Li, H. Wang, and G. Tao, "Current and future applications of distributed acoustic sensing as a new reservoir geophysics tool," *Open Petroleum Engineering Journal*, vol. 8, pp. 272–281, 2015.

[33] D. Miller, T. Parker, S. Kashikar, M. Todorov, and T. Bostick, "Vertical seismic profiling using a fibre-optic cable as a distributed acoustic sensor," in *Proceedings of the 74th EAGE Conference and Exhibition incorporating EUROPEC 2012*, Copenhagen, Denmark, Jun. 2012, p. 293.

[34] J. Mestayer *et al.*, "Field trials of distributed acoustic sensing for geophysical monitoring," in *SEG Technical Program Expanded Abstracts 2011*, Houston, TX, USA: Society of Exploration Geophysicists, 2011, pp. 4253–4257.

[35] A. Mateeva *et al.*, "Distributed acoustic sensing (das) for reservoir monitoring with vsp," *The Leading Edge*, vol. 32, pp. 1177–1300, 2013.

[36] A. Mateeva *et al.*, "Distributed acoustic sensing for reservoir monitoring with vsp," *The Leading Edge*, vol. 32, no. 10, pp. 1278–1283, 2013. DOI: 10.1190/tle32101278.1.

[37] A. Mateeva *et al.*, "Distributed acoustic sensing for reservoir monitoring with vertical seismic profiling," *Geophysical Prospecting*, vol. 62, no. 4, pp. 679–692, 2014. DOI: https://doi.org/10.1111/1365-2478.12116. eprint: https://onlinelibrary.wiley.com/doi/pdf/10.1111/1365-2478.12116. [Online]. Available: https://onlinelibrary.wiley.com/doi/abs/10.1111/1365-2478.12116.

[38] P. Webster, J. Wall, C. Perkins, and M. Molenaar, "Micro-seismic detection using distributed acoustic sensing," in *SEG Technical Program Expanded Abstracts 2013*, Houston, TX, USA: Society of Exploration Geophysicists, 2013, pp. 2459–2463.

[39] S. Karam *et al.*, "Microseismic applications using das," in *Proceedings of the 4th EAGE Passive Seismic Workshop*, Amsterdam, The Netherlands, Mar. 2013, p. 337.

[40] M. M. Molenaar, D. J. Hill, P. Webster, E. Fidan, and B. Birch, "First downhole application of distributed acoustic sensing for hydraulic-fracturing monitoring and diagnostics," *SPE Drilling & Completion*, vol. 27, no. 01, pp. 32–38, Mar. 2012, ISSN: 1064-6671. DOI: 10.2118/140561-PA. eprint: https://onepetro.org/DC/article-

pdf/27/01/32/3299307/spe-140561-pa.pdf. [Online]. Available: https://doi.org/10.2118/140561-PA.

[41] M. Molenaar, E. Fidan, and D. Hill, "Real-time downhole monitoring of hydraulic fracturing treatments using fibre optic distributed temperature and acoustic sensing," in *Proceedings of the SPE/EAGE European Unconventional Resources Conference and Exhibition*, Vienna, Austria, Mar. 2012.

[42] M. Molenaar and B. Cox, "Field cases of hydraulic fracture stimulation diagnostics using fiber optic distributed acoustic sensing (das) measurements and analyses," in *Proceedings of the SPE Unconventional Gas Conference and Exhibition*, Muscat, Oman, Jan. 2013.

[43] A. Bakulin, P. Golikov, R. Smith, K. Erickson, I. Silvestrov, and M. Al-Ali, "Smart das upholes for simultaneous land near-surface characterization and subsurface imaging," *Journal of Geophysics*, vol. 36, pp. 1001–1008, 2017.

[44] A. Hartog, M. Belal, and M. Clare, "Advances in distributed fiber-optic sensing for monitoring marine infrastructure, measuring the deep ocean, and quantifying the risks posed by seafloor hazards," *Marine Technology Society Journal*, vol. 52, pp. 58–73, 2018.

[45] Z. Broth and N. Hoult, "Field monitoring of rc-structures under dynamic loading using distributed fiber-optic sensors," *Journal of Performance of Constructed Facilities*, vol. 34, p. 04 020 070, 2020. DOI: 10.1061/(ASCE)CF.1943-5509.0001434.

[46] A. Brault and N. Hoult, "Assessment of reinforced concrete structures with distributed fibre optic sensors," in *Proceedings of the International Conference on Smart Infrastructure and Construction 2019 (ICSIC)*, Cambridge, UK, Jul. 2019, pp. 541–548.

[47] L. E. Kinsler, A. R. Frey, A. B. Coppens, and J. V. Sanders, *Fundamentals of Acoustics*, 4th. Wiley, 1999.

[48] B. A. Auld, *Acoustic Fields and Waves in Solids*. Krieger Publishing Company, 1990.

[49] M. Born and E. Wolf, *Principles of Optics*, 7th. Cambridge University Press, 1999.

[50] A. V. Oppenheim and A. S. Willsky, *Signals and Systems*. Prentice Hall, 1999.

[51] R. N. Bracewell, *The Fourier Transform and Its Applications*. McGraw-Hill, 2000.

[52] D. C. Ghiglia and M. D. Pritt, *Two-Dimensional Phase Unwrapping: Theory, Algorithms, and Applications*. John Wiley & Sons, 1998.

[53] R. C. Gonzalez and R. E. Woods, *Digital Image Processing*. Pearson, 2018.

[54] L. Cohen, *Time-Frequency Analysis*. Prentice Hall, 1995.

[55] C. R. Harris *et al.*, "Array programming with NumPy," *Nature*, vol. 585, no. 7825, pp. 357–362, 2020. DOI: 10.1038/s41586-020-2649-2.

[56] P. Virtanen *et al.*, "SciPy 1.0: Fundamental algorithms for scientific computing in python," *Nature Methods*, vol. 17, pp. 261–272, 2020. DOI: 10.1038/s41592-019-0686-2.

[57] W. McKinney, "Pandas: A foundational python library for data analysis and statistics," in *Python for High Performance and Scientific Computing*, 2011.

[58] J. D. Hunter, "Matplotlib: A 2d graphics environment," *Computing in Science & Engineering*, vol. 9, no. 3, pp. 90–95, 2007. DOI: 10.1109/MCSE.2007.55.

[59] C. G. Carr, C. M. Donahue, L. Viens, L. B. Beardslee, E. A. McGhee, and L. R. Danielson, "Detection of a space capsule entering earth's atmosphere with distributed acoustic sensing (das)," *Seismological Research Letters*, Feb. 2025, ISSN: 0895-0695. DOI: 10.1785/0220240394. eprint: https://pubs.geoscienceworld.org/ssa/srl/article-pdf/doi/10.1785/0220240394/7119019/srl-2024394.1.pdf. [Online]. Available: https://doi.org/10.1785/0220240394.